

## Automated Chemical Crystallography

Amy L. Fuller, Lindesay A. S. Scott-Hayward, Yang Li, Michael Bühl,  
Alexandra M. Z. Slawin,\* and J. Derek Woollins\*

*School of Chemistry, University of St Andrews, North Haugh, St Andrews, Fife, KY16 9ST U.K.*

Received January 18, 2010; E-mail: jdw3@st-andrews.ac.uk

**Abstract:** The first fully automated small-molecule robotic X-ray diffractometer is described. After demonstrating the utility of the instrument using multiple samples of ammonium bitartrate, we investigated the conformational chirality of diphenyl dichalcogenide ( $E_2Ph_2$ , where  $E = S, Se, \text{ or } Te$ ). Structural and computational studies suggest that the two enantiomers are energetically indistinguishable. Therefore, it was unsurprising that we found (in 35 suitable data collections) the proportion 0.51:0.49 of  $M$ - $S_2Ph_2$  to  $P$ - $S_2Ph_2$  in the bulk sample. Interestingly, after 65 data collections of  $Te_2Ph_2$ , (46 provided suitable data sets), we found the proportion  $0.72 \pm 0.13$  of  $M$ - $Te_2Ph_2$ , suggesting there could be a statistically significant preference for the  $M$ -enantiomer in the sample examined here. We found that  $Se_2Ph_2$  underwent homochiral crystallization, with all 24 crystals being  $M$ . Our experiments may represent a salutary lesson in statistical analysis.

### Introduction

Completely automated chemical crystallography has the potential to change the way crystallography is viewed. Knowledge of molecular shape is a key component in the understanding of molecular properties and reactivity. Chemists use mainly NMR and X-ray crystallography to determine the topology and stereochemistry of synthetic molecules. Recently, there have been rapid advances in these methods, enabling improvements in speed and precision. The most accurate and complete information comes from X-ray crystallography, which allows full 3-D information to be obtained in a matter of hours.<sup>1,2</sup> It is interesting to compare the progress in NMR spectroscopy with that of X-ray diffraction. In NMR, there was a step function improvement with the advent of Fourier transform techniques and superconducting magnets, which led to the ability to measure spectra rapidly, and within a decade, the use of autosamplers became routine in many laboratories. In crystallography, the use of charge-coupled device (CCD) detectors, covering an area in space and allowing many reflections to be measured simultaneously, has had a dramatic effect on the rate at which data can be collected but has not been matched by improvements in automation. Here we describe our progress in developing an automated system for chemical crystallography. The use of a robotic arm to exchange samples, along with automated software, enables full utilization of the data collection capability of a modern CCD laboratory-based X-ray diffractometer.

### Results and Discussion

In designing a fully automated X-ray diffractometer capable of continuous operation, our ultimate aim is to provide a system that, after submission of a crystalline sample, collects data

images, indexes the observed reflections to give a unit cell, optimizes the data collection strategy, integrates the observed data to give a reflection ( $hkl$ ) file, solves and refines the structure, and finally informs the sample submitter of the outcome. Clearly, approaching this level of automation for a large proportion of samples is very demanding and requires considerable development beyond the sample-changing automation available in macromolecular crystallography, but we have now accomplished this to a significant degree of success.

The diffractometer was constructed using a conventional CCD detector and goniometer with the addition of an electronic goniometer head (to allow for automatic centering of crystals), a robotic arm, and two drawers, each capable of holding 48 crystals mounted on magnetic pins. To enable sample mounting by inexperienced users, we chose to mount crystals on loops. The user(s) mount the crystals on loops with magnetic bases<sup>4</sup> and place them in one of the four sample trays. After this point the process is fully automated, right through to structure solution if requested. Using a robotic arm (which was originally developed for protein studies), the crystal is first transferred to the goniometer head and is then automatically centered. Crystals in chemical crystallography are usually grown with a diverse range of shapes, sizes, and colors. Previously available software for centering large, homogeneous and usually colorless protein crystals was not adequate for small-molecule crystal centering.

The development of new image recognition and centering software has enabled good crystal centering from a wide range of samples types. Successful centering is achieved in >90% of cases; some examples are shown in Figure 1. The established diffractometer control software was developed so after trial images have been taken, the unit cell is determined and the crystal quality ranked. The user can define a minimum quality so that if the ranking fails, it moves on to another crystal. However, if the rank passes then the data are collected and integrated, and subsequently the structure is determined using

(1) Massa, W. *Crystal Structure Determination*; Springer: Berlin, 2004; ISBN 3540206442.

(2) For a series of articles illustrating the power of X-ray diffraction see: Foundations of Crystallography, 60 years of Acta Crystallographica and the IUCr. *Acta Crystallogr. A* **2008**, *64* (Part 1), 1–271.

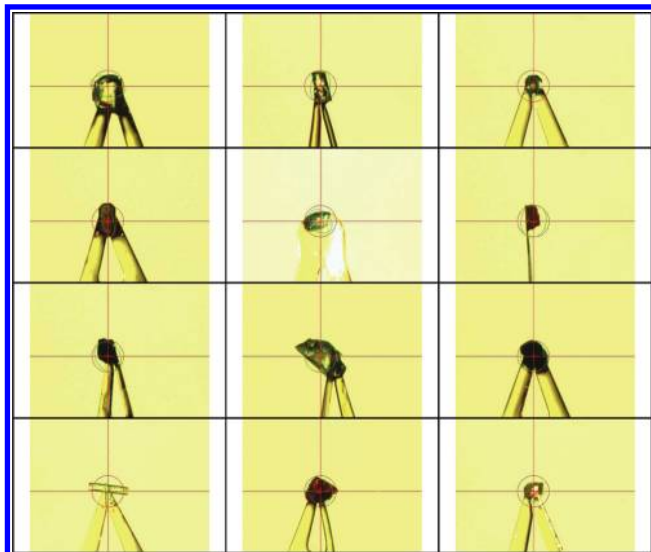


**Figure 1.** Examples of the outcome of automatic crystal centering using different size/shape crystals. The red circle represents the central portion of the X-ray beam.

the system STARRY<sup>3</sup> without human intervention. STARRY has been developed to run automatically all of the processes from Direct Methods solution through to refinement, utilizing relevant stand-alone crystallographic programs (currently programs from the SHELX family are used). The design philosophy is to imitate crystallographers' flexible thinking during structure development by using the indications from the refinement and structural knowledge, rather than relying on the proposed exact chemical formula. Finally, after structure solution and refinement, an e-mail alert is sent to the user reporting the data collection status. As a fallback, the data are also available for the users to return to if intervention is required, e.g., especially for a particularly difficult sample. The system has been developed sufficiently that it is now available commercially.<sup>4</sup>

As one test of the system, we mounted 24 different-sized crystals of ammonium bitartrate and collected data automatically. Of these 24 samples, 19 gave successful structure determinations without any user intervention (Table 1). The results indicate good-quality results from a range of crystals with fair  $R_{\text{int}}$  and  $R_1$  values. We have further tested our system with >1500 samples ranging from organic molecules through coordination chemistry compounds to "inorganic solids", such as coordination polymers and aluminum phosphates.

Typically we obtain ca. 80% success in acquiring useful  $hkl$  files from the fully automated sample collections, with a somewhat lower success rate for full automated structure determination. In continuous operation, for "normal" CCD quality/size crystals, we are able to collect and process up to 20 full data sets per 24 h.

This increase in throughput is leading to a different philosophy in how we use X-ray crystallography. Since we can now quite easily obtain 6–10 structures overnight, it is possible to use this equipment as an analytical as well as a structural tool. Furthermore, the ability to collect several data sets means we

**Table 1.** Selected Parameters from a Study of Ammonium Bitartrate Crystals,  $[\text{NH}_4][\text{C}_4\text{H}_5\text{O}_6]^\text{a}$

ID	rank	$R_{\text{int}}$	total no. reflns	no. unique reflns	no. obsd reflns	$R_1$
01	218	0.059	2375	1290	1227	0.065
04	214	0.061	3012	1310	1288	0.053
05	191	0.041	2252	1269	1245	0.057
06	216	0.167	2228	1272	1162	0.125
07	214	0.058	2558	1263	1193	0.09
09	217	0.033	2210	1228	1183	0.058
10	198	0.14	2152	1286	1259	0.089
12	189	0.11	4051	1308	1279	0.067
14	201	0.024	2312	1239	1217	0.048
15	211	0.041	2587	1271	1190	0.066
16	209	0.047	2383	1287	1215	0.063
17	203	0.041	2799	1271	1254	0.053
18	215	0.050	3092	1245	1212	0.056
19	205	0.036	2585	1279	1249	0.054
20	195	0.085	1808	1143	1122	0.069
21	186	0.038	2267	1266	1242	0.050
22	222	0.046	2198	1274	1250	0.057
23	201	0.078	2258	1267	1215	0.066
24	209	0.078	2415	1300	1214	0.075

<sup>a</sup> All data were collected at 125 K. The molecule crystallises in the orthorhombic space group  $P2_12_12_1$ . Typical standard uncertainties of cell parameters 0.002–0.003 Å. Values are for data as automatically processed, agreement factors are for a model with no hydrogen atoms, and all non-hydrogen atoms were refined with anisotropic thermal parameters. Supplementary Table 1 (Supporting Information) contains details of crystal dimensions.

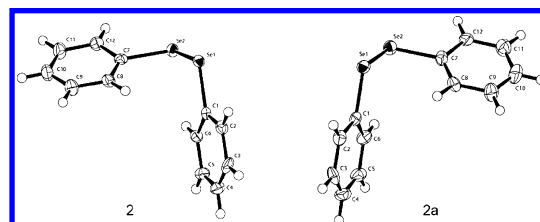


**Figure 2.** X-ray structures of *P*-Se<sub>2</sub>Ph<sub>2</sub> (**2**) and *M*-Se<sub>2</sub>Ph<sub>2</sub> (**2a**). The S and Te analogues are isomorphous.

can measure several crystals of a particular compound and then rank them competitively before collecting the best data set, or automatically test for polymorphism and/or test enough crystals to ensure that the chosen crystal is "typical". This ultimately improves data quality with very efficient use of both operator and diffractometer time.

One common occurrence in single-crystal studies is the determination of a structure with a particular absolute configuration from a single crystal without any evidence that this crystal is "typical". To further test the abilities of our robotic system, we investigated the usefulness of single-crystal studies for the determination of the crystallographic enantiomeric excess in PhEPh (E = S, Se, or Te). There was some low-resolution data available on these compounds,<sup>5</sup> but as a starting point we crystallographically characterized both *M*- and *P*-enantiomers of each compound in the E<sub>2</sub>Ph<sub>2</sub> series (Supplementary Tables 2 and 3, Supporting Information; Figure 2). The six structures are isomorphous. Unsurprisingly, the E–E bond lengths increase as the chalcogen size increases, from S (2.0260(14), 2.0289(7) Å) to Se (2.3066(7), 2.3073(10) Å) to Te (2.7089(7), 2.7073(5) Å), and are statistically indistinguishable between the *P*- and *M*-enantiomers of the same chalcogen.

(3) Li, Y.; Slawin, A. M. Z. St Andrews, Rigaku, Robotic by Yang (STARRY). This software uses a new set of algorithms loosely based on System Y, which was briefly reported: Hursthouse, M. B.; Light, M.; Li, Y. *Acta Crystallogr.* **2004**, *A60*, s81.

(4) For a video of this system in operation, see <http://www.rigaku.com/automation/actor-sm.html>, which illustrates the design described here.

(5) PhSSPh: Lee, J. D.; Bryant, M. W. R. *Acta Crystallogr.* **1969**, *B25*, 2094–2101. PhSeSePh: Marsh, R. E. *Acta Crystallogr.* **1952**, *5*, 458. PhTeTePh: Llabres, G.; Dideberg, O.; Dupont, L. *Acta Crystallogr.* **1972**, *B28*, 2438.

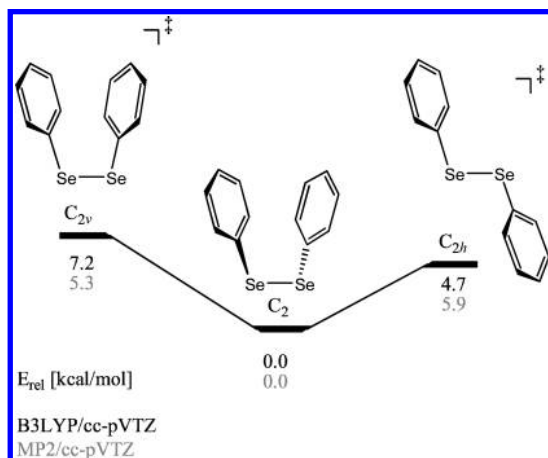


**Figure 3.** Results from  $\text{Se}_2\text{Ph}_2$  rotational barrier calculations (B3LYP/962(d)/6-31G\* geometries employed, see Supporting Information for details).

Logically enough, as the chalcogen atom size increases, the E–C bond distance also increases, and again, a negligible difference is seen between the enantiomers.

The E–E–C angles decrease across the series from S to Se to Te; however, there is a slight difference with the E(2)–E(1)–C(1) angle, which in every molecule is  $\sim 1\text{--}3^\circ$  larger than the E(1)–E(2)–C(7) angle. In  $\text{S}_2\text{Ph}_2$  and  $\text{Se}_2\text{Ph}_2$ , the similar E(1)–C(1)–C(2) and E(2)–C(7)–C(12) angles are much smaller than the E(1)–C(1)–C(6) and E(2)–C(7)–C(8) angles. In  $\text{Te}_2\text{Ph}_2$ , all four of these angles are similar. Finally, the torsion angles C(1)–E(1)–E(2)–C(7) in *P*- and *M*- $\text{Te}_2\text{Ph}_2$  are  $90.7(3)^\circ$  and  $-90.5(2)^\circ$ , respectively. The same torsion angles are slightly smaller ( $\sim 5^\circ$ ) in the sulfur and selenium analogues. With the knowledge that the individual enantiomers are structurally indistinguishable, other than the direction of their helicity, we investigated the energetic differences between the conformations. Rotational barrier calculations on free  $\text{Se}_2\text{Ph}_2$  resulted in one minimum where the molecule has  $C_2$  symmetry (the *M*- or *P*-enantiomer), as well as two transition states for rotation, with *syn*- and *anti*-conformations of the two phenyl groups (Figure 3). Both DFT and MP2 calculations predict a barrier on the order of 5–6 kcal/mol for the lower of the two transition states. This value is consistent with a previously calculated rotational barrier of 12 kcal/mol (at 204 K) for a bis(2,4,6-tri-*tert*-butylphenyl) diselenium derivative.<sup>6</sup> For  $\text{Te}_2\text{Ph}_2$ , a smaller rotational barrier than for  $\text{Se}_2\text{Ph}_2$  is expected, and the conversion barrier in the bis(2,4,6-tri-*tert*-butylphenyl) ditellurium derivative is 9.4 kcal/mol.<sup>7</sup>

As one would expect in the absence of a chiral environment, the *M*- and *P*-forms of the  $C_2$  minima are isoenergetic,<sup>9</sup> and our structural and computational studies confirm that these conformational enantiomers are indistinguishable. However, previous data (although limited) suggested that there could be

a preferential crystallization processes for these systems.<sup>8</sup> This phenomenon is not unknown, and Kondepudi et al.<sup>9</sup> studied (using optical examination of the products) the crystallization of aqueous sodium chlorate solutions, which gives D and L forms of solid  $\text{NaClO}_3$ , and noted that autocatalysis/nucleation plays an important role in determining the outcome. Stirred solutions underwent spontaneous resolution, having a clear preference for one hand or the other, while static solutions gave mixtures of D and L enantiomers. To produce statistically significant data in our experiments, we needed a large number of randomly chosen crystals. Crystals of commercially available samples were used, but we have not examined multiple batches. We used a simple Flack parameter test<sup>10</sup> as the criterion for handedness, though we recognize that there is the possibility of solid solutions causing some errors in this approach.

Forty-nine single crystals of  $\text{S}_2\text{Ph}_2$  were analyzed by X-ray crystallography. After data collection and integration, the structures were solved using direct methods and refined anisotropically, and the Flack parameter was closely examined. Of the 49 samples, 35 had Flack parameters and *R* factors of an appropriate quality to be reasonable for the determination of chirality. An analysis of these 35 samples showed that 18 crystals were the *M*-enantiomer.

The estimated proportion of *M*- $\text{S}_2\text{Ph}_2$  in the sample bottle,  $\hat{p}$ , can be found by using eq 1, where *M* is the total number of *M*-enantiomers and *X* is the total number of experiments. The estimated proportion of *M*- $\text{S}_2\text{Ph}_2$  in our sample bottle is 0.51. This nearly 50:50 ratio of *M*–*P*-enantiomers is consistent with the structural and computational data.

$$\hat{p} = \frac{M}{X} \quad (1)$$

Unfortunately,  $\text{Se}_2\text{Ph}_2$  was delivered as a powder. Recrystallization from  $\text{CH}_2\text{Cl}_2$  yielded yellow crystals, of which 24 single crystals were analyzed by X-ray diffraction. Out of the 24 crystals, 17 produced suitable data sets, all of these solved as the *M*-enantiomer. It appears that this sample, like those of Shimizu et al.,<sup>14</sup> underwent homochiral crystallization.

Finally, 65 single crystals of  $\text{Te}_2\text{Ph}_2$  were analyzed. Out of 46 good-quality data sets, 33 were *M*- $\text{Te}_2\text{Ph}_2$ . Using eq 1, the estimated proportion of *M*-enantiomers in our sample bottle is 0.72.

This result suggests that, in the sample analyzed here, there is an enantiomeric preference for *M*- $\text{Te}_2\text{Ph}_2$ , but the error in the experiment needs to be found. The error associated with the estimate,  $\hat{p}$ , is found through calculating a 95% confidence interval ( $\text{CI}_{95}$ ), which gives a range within which we are 95% certain that the true proportion of *M*- $\text{E}_2\text{Ph}_2$  in the sample bottle will lie. Since we have proportion data, a binomial distribution is used to calculate  $\text{CI}_{95}$  (eq 2). A binomial distribution usually applies when an experiment is repeated a fixed number of times. Each trial has one of two outcomes—success or failure—or in this case, *M*- $\text{E}_2\text{Ph}_2$  or not. The probability of success is the same for each trial, and the trials are statistically independent of each other. A summary of the results for the confidence intervals is shown in Table 2.

$$\text{CI}_{95} = \hat{p} \pm 1.96 \sqrt{\frac{\hat{p}(1-\hat{p})}{X}} \quad (2)$$

(10) Flack, H. D. *Chirality* **2008**, *20*, 681–690.

(6) Mario Pinto, B.; Leung, R. N. Y.; Sharma, D. *Magn. Reson. Chem.* **1988**, *26*, 729–734.

(7) Due to parity violation of the weak nuclear force, the respective enantiomers are not exactly isoenergetic but should differ slightly in energy. For  $\text{H}_2\text{Se}_2$  and  $\text{H}_2\text{Te}_2$ , for instance, this energy difference has been predicted to be on the order of 10–12 to 10–11 kcal/mol, i.e., undetectably small. See, e.g.: Berger, R.; van Wullen, C. *J. Chem. Phys.* **2005**, *122*, 134316–134318.

(8) Shimizu, T.; Isono, H.; Yasui, M.; Iwasaki, F.; Kamigata, N. *Org. Lett.* **2001**, *3*, 3639–3641.

(9) Kondepudi, D. K.; Kaufman, R. J.; Singh, N. *Science* **1990**, *250*, 975–976.

**Table 2.** Summary of  $CI_{95}$  for  $E_2Ph_2$  Experiments

	total	suitable	% <i>P</i> -	% <i>M</i> -	$CI_{95}$
$S_2Ph_2$	49	35	0.49	0.51	$\pm 0.17$
$Se_2Ph_2$	24	17	0	100	
$Te_2Ph_2$	65	46	0.28	0.72	$\pm 0.13$

<sup>a</sup> Delivered as a powder and recrystallized from  $CH_2Cl_2$ .

The  $CI_{95}$  for  $M-Te_2Ph_2$  is  $0.72 \pm 0.13$ , suggesting that there is a 95% chance that the true proportion of  $M-Te_2Ph_2$  in our sample bottle is within the interval 0.59–0.85. Most remarkably, we appear able to crystallize the selenium compound entirely as one isomer.

The  $CI_{95}$  for  $M-S_2Ph_2$  is  $0.51 \pm 0.17$ . These results, as we expected from our structural and computational studies, suggest that, in the sample bottle,  $S_2Ph_2$  crystallizes indiscriminately as either the *M*- or the *P*- enantiomer. This agrees with the expectation that there would be no noticeable preference for either enantiomer.

It is clear from the above that reported “chiral” crystal structures must be treated with some caution unless supported by other data. The crystallization of only one isomer of  $Te_2Ph_2$  is reminiscent of the experiments of Kondepudi and suggests autocatalysis/nucleation. These experiments highlight an important pedagogical issue with reproducibility in structural science, and we intend to expend further effort to assess how many duplicate measurements are needed in any particular situation.

In conclusion, using the *St Andrews Automated Robotic Diffractometer (STANDARD)*, the crystals can be mounted, images collected, and structures solved minimizing not only the time of the experiment but also the time required of a crystallographer. The developments we report suggest that single-crystal studies could become even more accessible, enabling higher quality data and multiple sampling for phase or chirality screening as well as being a valuable analytical tool.

## Experimental Section

Samples came from commercial sources, Aldrich Chemical Co. or Alfa Aesar.

The automated diffractometer<sup>4</sup> consists of a conventional sealed tube X-ray source (Mo radiation) equipped with graphite monochromator, Rigaku Saturn 724 CCD, AFC10 goniometer, Micoglide three-axis goniometer head, ACTOR Robotic arm, and X-Stream

LT device. Control software Cameraman<sup>11</sup> centers the crystal, while Director<sup>12</sup> provides input and inventory control over the samples. Two independent drawers fitted with two removable trays that each hold up to 24 samples means that the maximum capacity of the queueing system is 96 samples. The independent drawers can be loaded separately, thus enabling continuous operation. Director automatically starts CrystalClear<sup>13</sup> to control data collection, including indexing. If indexing results in a reasonable quality “ranking”, then the system goes on to collect a hemisphere of data either based on the indexed cell using a calculated strategy or using a standard data collection which is set up in the recipes. Once the data collection is underway, a second PC automatically integrates, Laue checks, absorption corrects, and outputs an *hkl* file. If so instructed, the second PC will also attempt a fully automated structure solution.<sup>14,15</sup> At the end of these processes, the sample submitter is sent an e-mail indicating the overall outcome.

To allow for the robotic mounting, magnetic bases are used. We used conventional nylon loops or laser-cut loops mounted on stainless steel pins from Mitegen ([http://mitegen.com/mic\\_catalog.php?c=MicroMounts](http://mitegen.com/mic_catalog.php?c=MicroMounts), [http://www.jenabioscience.com/cms/en/1/catalog/731\\_micromounts8482\\_19\\_mm.html](http://www.jenabioscience.com/cms/en/1/catalog/731_micromounts8482_19_mm.html)).

Experimental details for the  $E_2Ph_2$  samples are included in the Supporting Information.

**Acknowledgment.** We are grateful to the UK Engineering and Physical Sciences Research Council for support, to Russ Athay and Claire Wilson, and to Rigaku Americas software development and support. M.B. thanks EaStCHEM for support and access to the EaStCHEM Research Computing Facility maintained by Dr. H. Früchtl.

**Supporting Information Available:** Supplementary Table 1, crystal sizes and *R*-factors of automated data collections for ammonium bitartrate; Supplementary Table 2, details of data collections for **1–3**; Supplementary Table 3, selected bond lengths and angles for **1–3**; experimental details; X-ray diffraction data (CIF). This material is available free of charge via the Internet at <http://pubs.acs.org>.

JA100247Y

- (11) *Cameraman*; Rigaku Corp.: Tokyo, Japan, 2005.
- (12) *Director*, Version 3.0; Rigaku Corp.: Tokyo, Japan, 2009.
- (13) *CrystalClear*, Version 2.0; Rigaku Corp.: Tokyo, Japan, 2009.
- (14) *Crystal Structure*, Version 3.8, Single Crystal Structure Analysis Software; Rigaku/MS: The Woodlands, TX, 2006.
- (15) Sheldrick, G. M. *Acta Crystallogr.* **2008**, *A64*, 112–122.